
Numerical Analysis of the Lateral Response of Pile Foundations under Overall and Progressive Scour Conditions

[Binhui Ma](#)^{*}, Xiangrong Li, [Zengliang Wang](#), [Tian Lan](#), Xu Deng, Bicheng Du, Yarui Xiao, Long Peng, Yuqi Li

Posted Date: 27 February 2026

doi: 10.20944/preprints202602.1899.v1

Keywords: general scour; lateral behavior; pile-soil interaction; square and circular pile with same cross-sections; numerical analysis



Preprints.org is a free multidisciplinary platform providing preprint service that is dedicated to making early versions of research outputs permanently available and citable. Preprints posted at Preprints.org appear in Web of Science, Crossref, Google Scholar, Scilit, Europe PMC.

Copyright: This open access article is published under a [Creative Commons CC BY 4.0 license](#), which permit the free download, distribution, and reuse, provided that the author and preprint are cited in any reuse.

Disclaimer/Publisher's Note: The statements, opinions, and data contained in all publications are solely those of the individual author(s) and contributor(s) and not of MDPI and/or the editor(s). MDPI and/or the editor(s) disclaim responsibility for any injury to people or property resulting from any ideas, methods, instructions, or products referred to in the content.

Article

Numerical Analysis of the Lateral Response of Pile Foundations under Overall and Progressive Scour Conditions

Binhui Ma ^{1,2,3,*}, Xiangrong Li ¹, Zengliang Wang ^{1,2}, Tian Lan ^{1,2}, Xu Deng ¹, Bicheng Du ¹, Yarui Xiao ¹, Long Peng ¹ and Yuqi Li ¹

¹ School of Civil Engineering, Hunan University of Science and Technology, Xiangtan 411201, China

² Hunan Provincial Key Laboratory of Geotechnical Engineering for Stability Control and Health Monitoring, Xiangtan 411201, China

³ Engineering Testing Co., Ltd. of Hunan University of Science and Technology, Xiangtan 411201, China

* Correspondence: mbh@hnust.edu.cn; Tel.: +86-157-7322-7917

Abstract

Several finite element numerical simulations were conducted in this study to investigate the laterally loaded response of pile foundations under general scour conditions in clay, the finite element model was verified by centrifuge tests, and the “model change” method was used to simulate the formation process of general scour and its impact on the lateral bearing response of pile foundations. The effects of overall scour and progressive scour on the load-displacement relationship, pile-soil deformation and failure mode, bending moment, displacement of circular and square pile foundations with equal cross-sectional areas under the same scour depth were analyzed. The results show that under no scour and two general scour conditions, the lateral bearing capacity of square-section pile foundations is higher than that of circular pile foundations with equal cross-sections; the general scour changes the pile-soil deformation and failure mode of laterally loaded pile foundations and reduces the wedge-shaped failure zone of soil around the pile; the wedge-shaped failure area of the soil around laterally loaded square cross-section piles is larger than that of circular cross-section piles of equal cross-sectional area; when the scour depth is the same, one overall scour and progressive scour have less impact on the lateral bearing capacity of the pile foundation; under the same scour depth conditions, one overall scour and distribution scour have less impact on the lateral bearing capacity of the pile foundation.

Keywords: general scour; lateral behavior; pile-soil interaction; square and circular pile with same cross-sections; numerical analysis

1. Introduction

Pile foundations are widely adopted for major over-water infrastructure, such as bridge piers, offshore wind turbines and coastal terminals, because they provide high axial and lateral capacity, strong resistance to overturning, and can be installed efficiently with a relatively small construction footprint [1–7]. In these settings, capacity design must account for the combined action of gravity loads transmitted from the superstructure and lateral demands induced by currents, waves and wave-current interactions, which often govern serviceability through deflection and bending demands as much as ultimate strength [4,8–11]. The problem is further complicated by hydrodynamic, geotechnical coupling: flow-soil-pile interactions generate complex turbulent structures around the foundation, including downflow, horseshoe vortices and wake vortices [12–16]. These vortical systems intensify near-bed shear stresses, mobilise sediment, and progressively excavate the shallow bed material to form scour holes. By removing overburden and lateral confinement near the mudline, scour reduces the effective embedment and shifts the load transfer

mechanism, typically increasing pile head flexibility and amplifying bending moments and shear forces in the upper portion of the pile [17–21]. As a result, pile capacity can be markedly degraded, with lateral resistance often affected most severely, particularly for pile groups where shadowing effects, interaction between front and rear piles, and non-uniform scour geometries can lead to highly asymmetric load sharing [22–26]. These coupled processes motivate systematic investigation of pile (and pile-group) behaviour under scour, with explicit attention to both hydrodynamic forcing and the evolving seabed/riverbed morphology that controls the soil resistance mobilised during lateral loading [27–32].

At present, research on pile-foundation scour and its implications for bearing capacity can be broadly grouped into two strands. The first focuses on the mechanisms of scour. Scour is commonly classified as general scour (reach-scale degradation of the riverbed within a certain depth range), local scour (sediment removal around a pile or pier caused by flow obstruction and the associated acceleration and vortex action, forming a local scour hole), and contraction scour (bed erosion triggered by an abrupt reduction in channel cross-section that increases flow velocity) [23,33–35]. Scour removes soil from around the foundation, thereby reducing the effective embedment depth, increasing the load eccentricity (lever arm) and structural demand, and ultimately degrading pile capacity; among these factors, scour depth is often identified as the dominant parameter governing the loss of pile bearing capacity [36,37]. Field evidence further suggests that scour is a primary contributor to failures of bridges crossing waterways: in China and the United States, bridge damage attributed to scour and flooding has been reported to account for approximately 80% and 60% of cases, respectively, whereas earthquake-induced failures represent only about 2% [38,39].

The second strand addresses pile capacity under scour conditions. Under lateral loading, pile-soil interaction is often governed by wedge-type failure of the shallow soil around the pile, making the lateral capacity particularly sensitive to scour. In current engineering practice, lateral design under scour commonly follows codified approaches such as FHWA-DS, FHWA-DP, and API methods [40,41]. The FHWA-DP approach assumes that the effective stress state around the pile is not altered by scour, whereas the FHWA-DS and API formulations can account for scour-induced stress changes in the surrounding soil. However, these methods are generally formulated for single piles under a prescribed (fixed) scour geometry and do not capture the evolving soil stress history associated with scour-hole development. Complementary experimental and numerical efforts have therefore been undertaken. Qi et al. [42] used centrifuge modelling to quantify the effect of local scour on the lateral capacity of piles in sand, while Chortis et al. [43] examined the influence of scour depth on the capacity of a single pile in centrifuge tests. Using finite-element analyses, Wang et al. [44,45] investigated the evolution of lateral resistance of pile groups under local scour in both sand and clay. Lin et al. [46,47] further derived an expression for the vertical effective stress around piles based on the Boussinesq point-load solution and proposed a corresponding modification to the API method for piles in sand.

After scour is completed, the remaining (unscoured) soil around the pile becomes overconsolidated, and both its stress history and hydro-mechanical properties are altered. Most centrifuge studies on lateral pile behaviour under scour adopt a pre-excavated scour-hole configuration, which cannot reproduce the changes in soil stress history and material parameters induced by the scour process. By contrast, many theoretical treatments rely on simplified elastic idealisations that depart substantially from real soil behaviour. Existing numerical studies also commonly “instantaneously” impose the scour hole in a single step, thereby neglecting the fact that scour develops progressively and can imprint an evolving stress path on the surrounding soil. In addition, prior work has largely focused on piles with circular cross-sections.

Here we address these gaps using finite-element modelling of scour capacity coupling for pile foundations in clay. The soil response is captured with a modified Cam-Clay constitutive model. For a given target scour depth, we quantify lateral load behaviour under two idealisations: instantaneous (one-step) scour and progressive scour. We further compare the lateral capacity of square and circular

piles with the same cross-sectional area under general scour conditions. The results provide practical guidance for the design of pile foundations in scour-prone environments.

2. Finite Element Model Description

Existing studies provide no centrifuge or field test data that directly quantify the lateral load capacity of piles in clay under general scour conditions. Therefore, the finite-element (FE) model developed in this study was validated against the centrifuge test results reported by Ilyas (2004) [48] for laterally loaded piles in clay. The experiments were conducted at an acceleration level of 70g using normally consolidated kaolin clay, and the basic physical and mechanical properties of the clay are summarised in Table 1. The model pile was fabricated from a hollow aluminium tube with a square cross-section, with a width of 12 mm, corresponding to a prototype pile width of 0.84 m based on centrifuge scaling laws. The model pile length was 260 mm (prototype 18.2 m), with an embedment depth of 210 mm (prototype 14.7 m). The pile bending stiffness was $E_m I_m = 384 \text{ kN}\cdot\text{cm}^2$, equivalent to 922 MNm^2 at the prototype scale. The clay layer thickness was 245 mm (prototype thickness 17.15 m). Further details of the experimental setup, loading procedure, and test programme are available in Ilyas (2004) [48].

Table 1. Parameters of physical properties of kaolin clay.

Parameters of kaolin clay	Parameter Value
Unit Weight (γ)	16kN/m ³
Water Content	66%
Liquid Limit	79.8%
Plastic Limit	35.1%
Compression Coefficient(C_c)	0.55
Rebound Coefficient(C_s)	0.14
Permeability Coefficient (k)	$2 \times 10^{-8} \text{ m/s}$
Undrained Shear Strength at 15m Depth (Prototype)	20kPa
Undrained Shear Strength at 0m (Prototype)	0kPa

3. Material Parameters and Constitutive Model

In the finite-element (FE) modelling, the Modified Cam–Clay (MCC) model was employed to represent the stress–strain behaviour of the kaolin clay. The MCC parameters for kaolin were adopted from the studies of Ilyas (2004) [48] and Wang et al. (2022) [44], including the slope of the normal consolidation line $\lambda = C_c / 2.3 = 0.239$, the slope of the unloading–reloading line $\kappa = C_s / 2.3 = 0.061$, the slope of the critical state line $M = 6 \sin \phi' / (3 - \sin \phi') = 1.07$, and the critical-state friction angle $\phi' = 26.9^\circ$. According to the MCC formulation, the initial void ratio of the clay varies with depth as:

$$e_0 = e_1 - \lambda \ln \left(\frac{q^2}{M^2 p'} + p' \right) + \kappa \ln \left(\frac{q^2}{M^2 p'^2} + 1 \right) \quad (1)$$

where p' is the mean effective stress, q is the deviatoric stress, $e_1 = 2$.

The model treated the pile as an elastic material with the elastic modulus of 22.2 GPa and the Poisson's ratio of 0.2.

4. Finite Element Model Setup

Considering the symmetry of the laterally loaded pile foundation model, a symmetric FE model was adopted. To eliminate boundary effects, the soil domain was set to $34D$ in the x -direction and $13D$ in the y -direction, and the distance from the pile tip to the bottom boundary was $15D$ [31]. Figure 1 shows a representative FE mesh model used in this study. The FE analysis consisted of four steps:

(i) Initial geostatic stress step. To reproduce the in-situ stress state of the soil, the lateral boundaries were constrained in the x -direction, and the ground surface was restrained in the x -, y -, and z -directions. The two faces perpendicular to the vertical loading direction were assigned a y -direction displacement constraint and a symmetry boundary condition, respectively. Gravity and an initial stress field were applied to establish the in-situ geostatic stress state. The at-rest earth pressure coefficient was $K_0 = 1 - \sin \phi' = 0.4$.

(ii) The model pile was installed using the “wish-in-place” approach, and the pile–soil interface properties were specified accordingly. The tangential and normal contact behaviours were defined using the Coulomb friction formulation in ABAQUS. Following Wang et al. [31], the friction coefficient of 0.32 was assigned to the pile–soil interface [49]. Hard contact was adopted in the normal direction with separation allowed, and gravity was applied to the pile.

(iii) The “Model Change” technique in the finite-element software was used to deactivate the soil elements within the prescribed scour depth, thereby simulating the formation of a general scour hole and capturing the soil stress history and the associated evolution of its physical and mechanical properties during scour. For the model-validation stage, this step was not implemented to ensure consistency with the centrifuge tests; the comparison was used to assess the validity and accuracy of the FE model.

(iv) The displacement-controlled lateral load was applied to the model pile at the loading point, in the direction of the symmetry plane in the model. The pile surface was kinematically coupled to a single reference (loading) point, and the lateral displacement was imposed at this point to facilitate extraction of the numerical results.

The mesh convergence analysis was performed for the FE simulations. Doubling the mesh density led to a change of less than 3% in the computed load-displacement response. The FE model shown in Figure 1 comprises 69,868 elements.

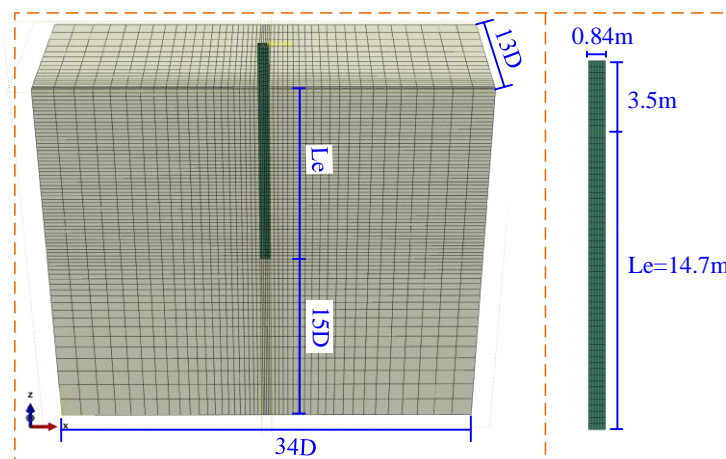


Figure 1. Finite element model mesh for centrifuge comparison.

5. Comparison of Finite Element Results and Centrifuge Tests

Figure 2 presents a comparison between the pile-head load-displacement response predicted by the FE model and that measured in the centrifuge tests. Overall, the numerical predictions reproduce the experimental trend well over the full loading range, including the initial stiffness and the subsequent non-linear softening as displacement increases. The close agreement indicates that the adopted constitutive description and pile-soil interface modelling are capable of capturing the key mechanisms governing the lateral response of the pile in clay. According to the API guideline for laterally loaded piles, the ultimate condition can be defined when the lateral displacement at the mudline reaches $0.1D$ [40]. The FE model yields a response consistent with this criterion and the corresponding centrifuge observations, thereby confirming the accuracy and reliability of the proposed FE modelling framework for subsequent parametric analyses.

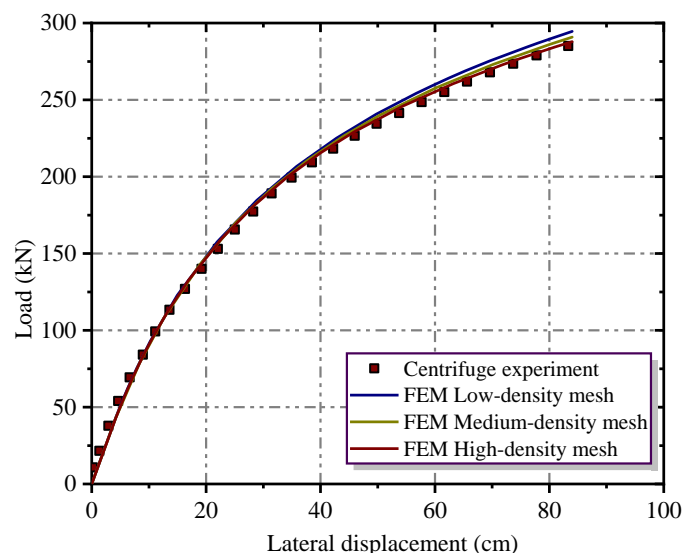


Figure 2. Comparison of finite element results and centrifuge tests.

Figure 3 compares the bending moment-depth profiles obtained from the centrifuge tests and the FE simulations at four prescribed pile-head lateral displacements ($0.05D$, $0.1D$, $0.3D$ and $0.4D$, where D is the pile displacement/diameter). Overall, the FE model reproduces the centrifuge measurements well across all displacement levels, capturing both the magnitude and the shape of the moment distributions. As the pile-head displacement increases from $0.05D$ to $0.4D$, the bending moment increases markedly and the moment profile becomes broader, indicating progressive mobilisation of soil resistance over a larger depth range. The bending moment rises from the pile head to a distinct maximum located at an intermediate depth (approximately 6–8 m below the mudline), and then decays towards the pile toe, consistent with the development of a rotation point and deeper fixity. The peak moment increases systematically with displacement, reaching on the order of 1.8–1.9 MN·m at $0.4D$. Minor deviations between the FE and centrifuge data occur locally (typically near the peak-moment zone), but the agreement remains close, confirming that the validated FE model can reliably predict the pile bending demand and its evolution with increasing lateral deformation.

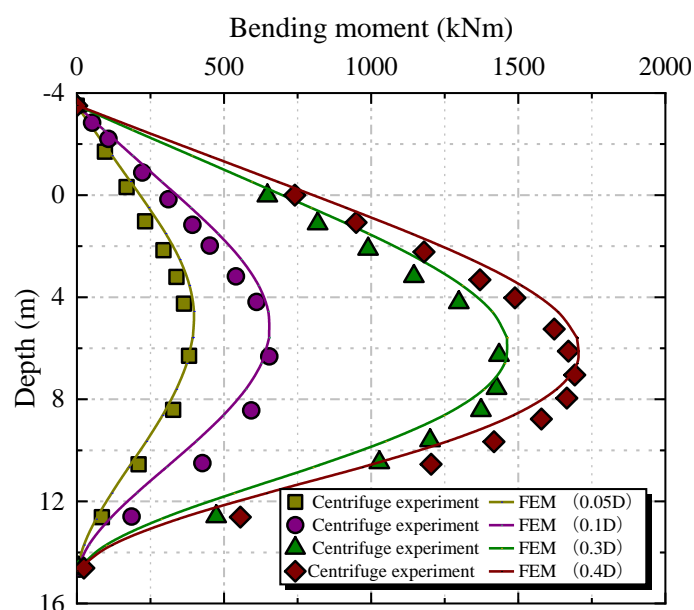


Figure 3. Comparison of finite element results and centrifuge tests for bending moment-depth curves.

6. Finite Element Results Analysis

In this section, a parametric study was carried out to compare the lateral behaviour of square and circular piles with the same cross-sectional area, so that the influence of pile shape could be isolated from the effect of axial area. The pile-soil interaction under horizontal loading was examined under three representative conditions: (i) an unscoured baseline case, (ii) general scour to 2.5 m developed progressively by removing the soil in five increments of 0.5 m (corresponding to the coloured region in Figure 3(b)), and (iii) an instantaneous (one-step) scour in which the full 2.5 m of soil was removed at once (as indicated by the red region in Figure 3(a)). The progressive-scour scheme was introduced to account for the evolution of soil stress history during scour development, whereas the one-step scour represents the common idealisation adopted in conventional modelling. The FE models used in Figure 4 comprise 93,890 and 104,670 elements, respectively.

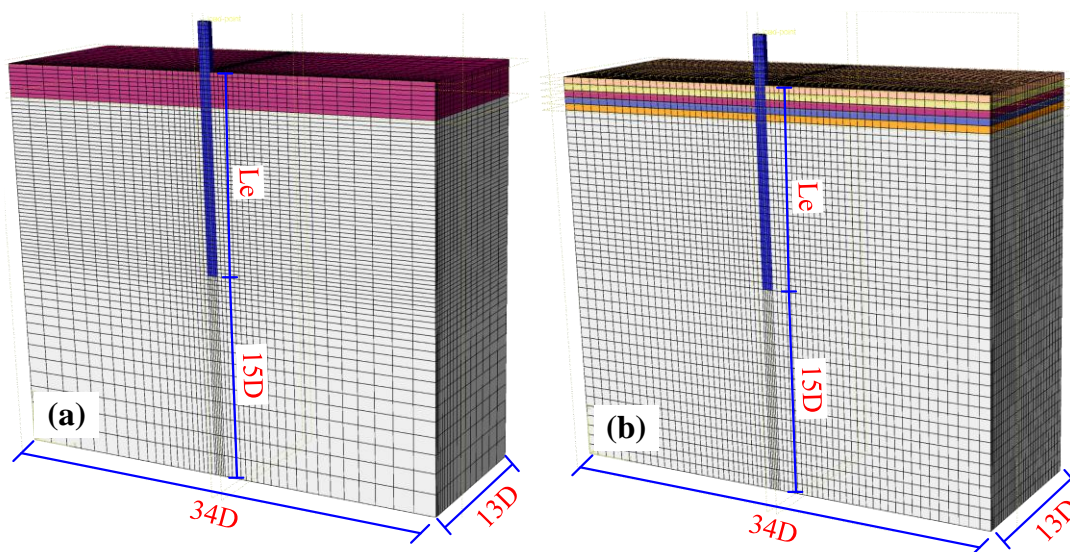


Figure 4. Finite element mesh model under general scour, (a) overall scour; (b) progressive scour.

Figure 5 compares the load-displacement responses of square and circular piles with the same cross-sectional area under three conditions: unscoured, overall (one-step) scour, and progressive (staged) scour. For a given scour depth in clay, the curves obtained from the overall scour and staged scour simulations are almost coincident, indicating that within the investigated range, the method used to impose scour (instantaneous versus incremental removal) has a minor influence on the lateral load-displacement relationship of the pile. At a pile-head lateral displacement of 30 cm, the lateral capacity of the square pile and the equal-area circular pile under unscoured conditions is 208.32 kN and 184.57 kN, respectively. Under staged scour, the corresponding capacities decrease to 146.08 kN (square) and 124.67 kN (circular), highlighting the pronounced degradation in lateral resistance induced by scour. Across both scour and unscoured cases, the square pile consistently mobilises a higher lateral resistance than the circular pile. Quantitatively, relative to the circular pile, the square pile provides an increase in lateral capacity of approximately 13% in the unscoured condition and 17.7% under scour. These results suggest that, for piles with an equal cross-sectional area, modifying the pile cross-sectional shape (from circular to square) can be an effective means of enhancing lateral load capacity, offering a practical design option for improving performance in scour-prone environments.

Figure 6 shows the horizontal displacement contours (U_1) of the laterally loaded square pile-soil system under unscoured (Figure 6a) and scoured (Figure 6b) conditions. Compared with the unscoured case, general scour leads to a progressive deepening of the wedge-type deformation/failure zone around the pile, indicating that the mobilised soil resistance is transferred to deeper layers as the near-surface confinement is removed. Meanwhile, the extent of the actively

compressed (passive) soil zone in front of the pile becomes smaller after scour, reflecting the reduced availability of shallow soil to provide lateral support. Scour also increases the pile deformation above the post-scour mudline: the horizontal displacement of the pile segment exposed above the bed becomes more pronounced, and a clearer “kick-out” (toe deflection) develops near the pile tip, suggesting enhanced pile rotation and a shift of the rotation point. These trends can be primarily attributed to the fact that general scour reduces the effective embedment depth and increases the load eccentricity of the lateral action, thereby weakening the lateral confinement provided by the shallow soil and amplifying pile deflection and rotation. For the same pile-head displacement, the pile displacement at the mudline after scour is larger than that at the corresponding depth in the unscoured case, and the wedge-type deformation zone extends further downward. This phenomenon becomes increasingly evident with increasing scour depth, highlighting that the shallow clay strata contribute disproportionately to lateral resistance; once removed by scour, the lateral load-carrying capacity of the pile can be substantially reduced.

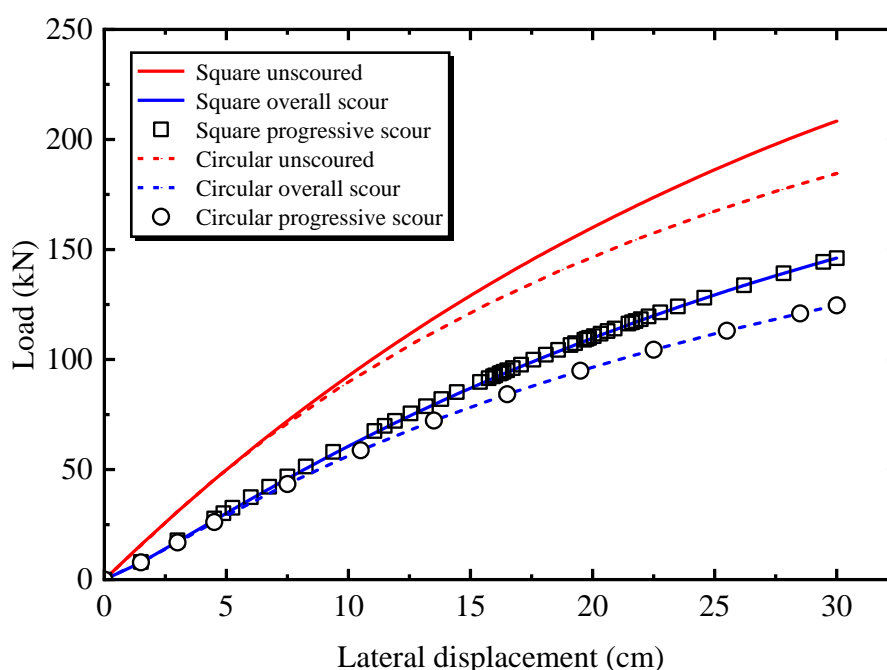


Figure 5. Comparison of load-displacement relationships of circular and square cross-section pile foundations under different scour conditions with equal cross-sectional areas.

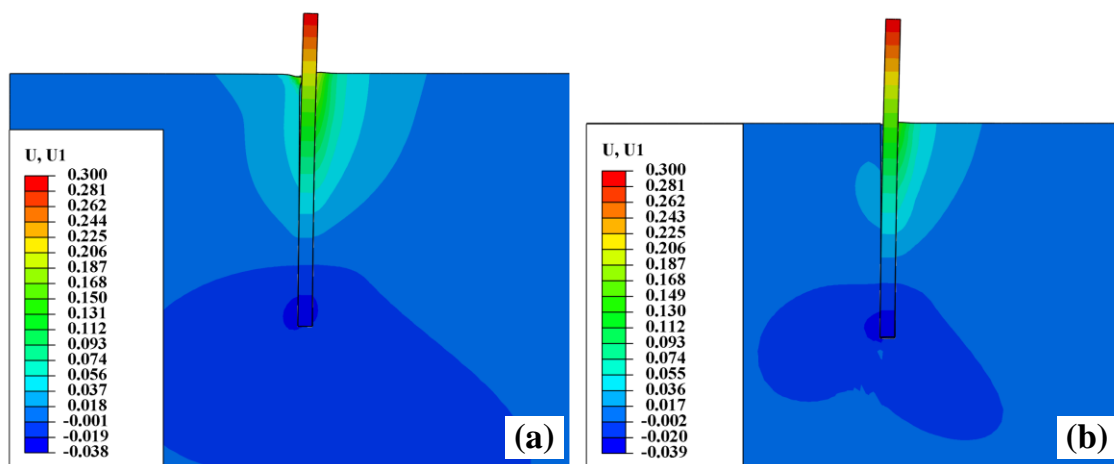


Figure 6. Pile-soil displacement profiles of square cross-section piles before and after scour.

Figure 7 presents the horizontal displacement contours (U_1) of the pile-soil system at the post-scour mudline under general scour, comparing the square (Figure 6a) and circular (Figure 6b) piles with equal cross-sectional area. For both pile shapes, a pronounced wedge-shaped deformation zone develops around the pile under lateral loading. As the distance from the pile increases, the displacement magnitude decays gradually and the affected region transitions from a highly deformed zone to a weakly deformed zone, allowing the surrounding soil to be conceptually divided into a plastic zone, an elastic zone, and an essentially undisturbed zone. Within the plastic zone, the displacement field around the square pile exhibits a more blocky/rectangular pattern over a limited area, consistent with the presence of flat pile faces that impose directional kinematic constraints on the adjacent soil. Moreover, along the loading direction, the square pile mobilises a noticeably larger wedge-shaped soil mass than the circular pile. In contrast, the soil behind the pile shows negligible horizontal displacement for both sections, indicating limited mobilisation in the wake region under the considered loading and boundary conditions. These observations suggest that, under both scoured and unscoured conditions, a laterally loaded square pile engages a larger volume of surrounding soil than an equal-area circular pile, thereby mobilising greater passive resistance. This larger mobilisation zone provides a mechanistic explanation for the consistently higher lateral capacity of the square pile observed in the load-displacement responses.

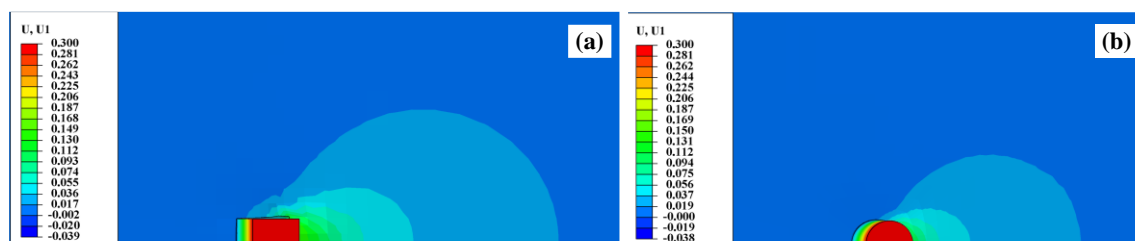


Figure 7. Pile-soil displacement profile at mud surface of square cross-section pile under general scour conditions.

Figure 8 shows the bending moment-depth profiles of the pile under three prescribed pile-head lateral displacements (0.1 m, 0.2 m and 0.3 m) for three conditions: unscoured, overall (one-step) scour, and progressive (staged) scour. For both the square- and circular-section piles, the unscoured case consistently exhibits larger bending moments than the scoured cases at the same depth, indicating that under displacement-controlled loading, the pile mobilises a higher lateral reaction (and thus larger bending demand) when the near-surface soil confinement is intact. In contrast, scour reduces the available shallow resistance and leads to a smaller bending response throughout the upper portion of the pile. The overall scour and progressive scour results are nearly indistinguishable for all displacement levels, suggesting that explicitly modelling the staged scour process produces only marginal differences in the predicted bending-moment distribution compared with the common one-step scour idealisation (for the scour depth considered). Notably, scour causes the location of the maximum bending moment to migrate downwards, reflecting a deeper mobilisation of soil resistance and a shift in the effective fixity/rotation region. When the scour depth reaches 2.5 m, the depth of peak moment increases by approximately 0.4 m for the square pile and 0.7 m for the circular pile relative to the unscoured condition. At the largest imposed pile-head displacement (0.3 m), the peak bending moments for the square and circular piles are 1404.31 kN·m and 1335.33 kN·m in the unscoured case, decreasing to 1124.91 kN·m and 1021.06 kN·m under scour, respectively. Overall, the square pile develops a higher peak bending moment than the equal-area circular pile by about 5% (unscoured) and 10% (scoured), implying that adopting a square cross-section can mobilise greater lateral resistance, and hence a higher lateral load-carrying capacity particularly under scour conditions.

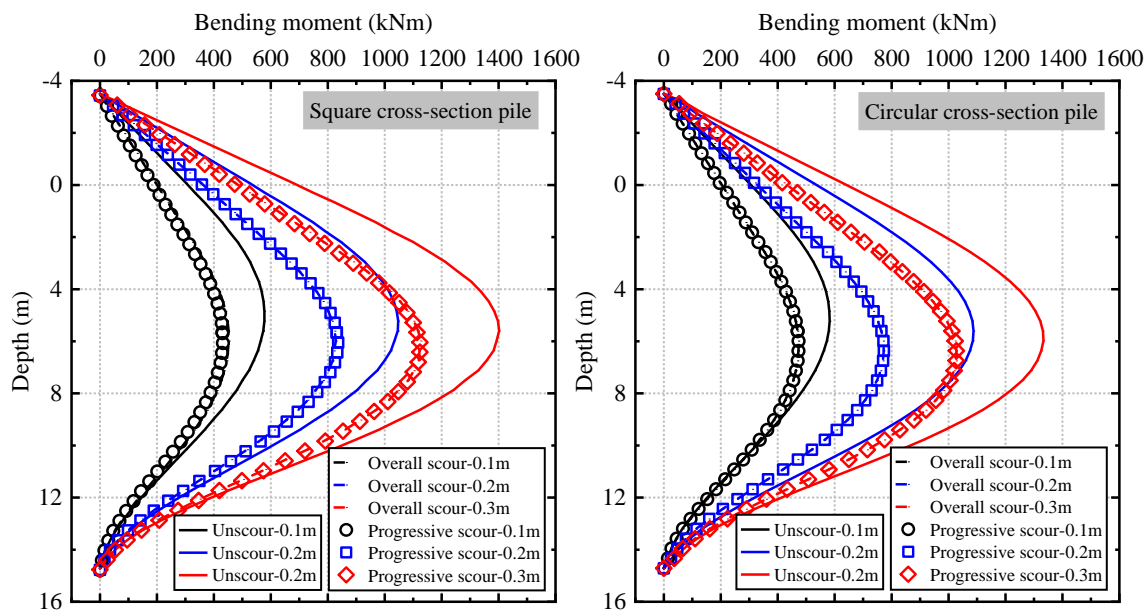


Figure 8. Bending moment-depth distribution of piles under different displacement loads in three conditions: (a) square cross-section pile; (b) circular cross-section pile.

Figure 9 shows the pile lateral displacement-depth profiles under three prescribed pile-head displacements (0.1 m, 0.2 m and 0.3 m) for three conditions: unscoured, overall (one-step) scour, and progressive (staged) scour, for both the square- and circular-section piles. For a given pile-head displacement, the difference between the scoured and unscoured displacement profiles varies with depth: as depth increases, the discrepancy first increases and then decreases, indicating that scour most strongly modifies pile deformation within an intermediate depth range rather than uniformly over the entire embedded length. This depth-dependent trend becomes more pronounced as the imposed pile-head displacement increases, reflecting progressively stronger nonlinearity and mobilisation of soil resistance with larger lateral deformation. Despite the clear influence of scour on the magnitude and shape of the displacement profiles, the depth of the zero-displacement point is only weakly affected by scour for the investigated cases. This suggests that, under displacement-controlled loading, scour primarily amplifies pile deformation above and near the mudline, while the position of the rotation point remains relatively stable. In addition, compared with the circular pile of equal cross-sectional area, the square pile exhibits a shallower zero-displacement depth, implying a more pronounced near-surface rotation and a different distribution of bending and soil reaction along the pile. Overall, the results highlight that pile cross-sectional shape influences the deformation mechanism and the depth-wise mobilisation of soil resistance under scour conditions.

Figures 10–15 compare the p - y curves at five depths below the post-scour mudline (1, 2, 3, 4, and 5 m) for equal-area circular (C) and square (S) piles under three conditions: unscoured, overall scour, and progressive scour. In the p - y curves, the soil reaction p was derived from the bending moment-depth profiles obtained from the FE analyses at each prescribed lateral displacement level. Each moment-depth profile was first fitted using a fourth-order polynomial [50], and the corresponding soil reaction-depth relationship was then obtained by taking the second derivative of the fitted function. It should be noted that the depths shown in Figures 10–15 are defined at the same pile-length position measured from the pile tip. Therefore, for the unscoured case, the thickness of overburden soil equals the post-scour mudline depth plus the scour depth.

It can be observed that, at a given depth, the soil reaction in the unscoured case is consistently higher than that in the two scour cases at the same imposed lateral displacement. This reflects the loss of near-surface confinement and the reduction in effective embedment caused by scour, which weakens the mobilised subgrade reaction in the upper soil layers. The influence of scour is most pronounced at shallow depths, whereas the discrepancy between the unscoured and scoured

responses gradually diminishes with increasing depth below the post-scour mudline, indicating that the deeper soil retains a broadly similar stress state and continues to provide comparable resistance.

For a fixed pile cross-section, the overall scour case yields slightly lower soil resistance than the progressive scour case, although the differences remain modest across the displacement range considered. This suggests that, for the investigated clay and scour depth, the stress-history effects associated with incremental scour development have a secondary influence on the resulting p - y response compared with the dominant geometric effect of removing the overburden. In addition, under the same loading and scour condition, the square-section pile consistently mobilises a higher soil reaction than the equal-area circular pile. This behaviour indicates a greater mobilisation of passive resistance in front of the pile and a larger engaged soil wedge, which translates into enhanced lateral stiffness and capacity. Overall, the comparisons confirm that modifying the pile cross-sectional shape from square to circular can improve the lateral load-carrying performance under unscoured, overall scour, and progressive scour conditions.

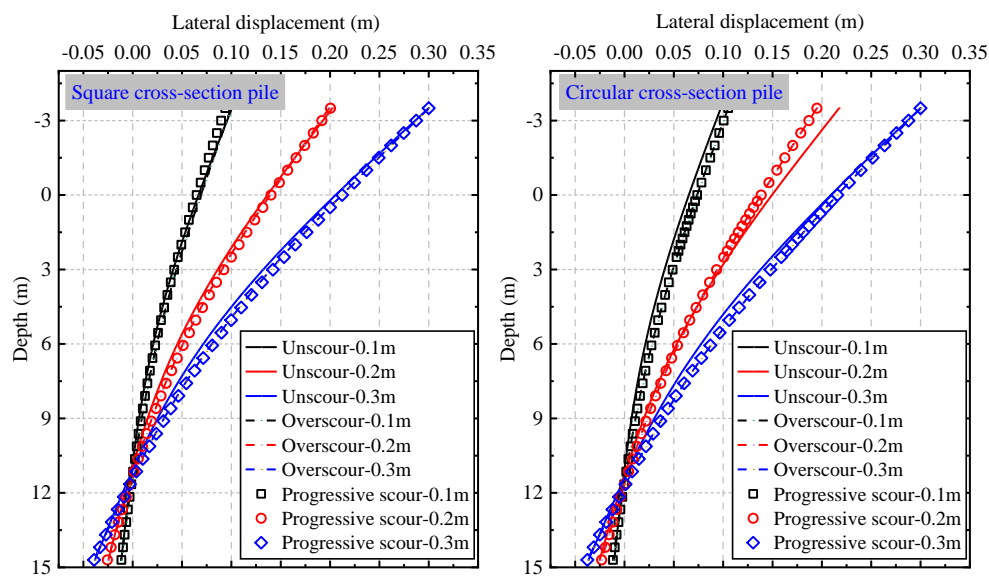


Figure 9. Displacement-depth distribution of piles under different displacement loads in three conditions: (a) Square cross-section pile; (b) Circular cross-section pile.

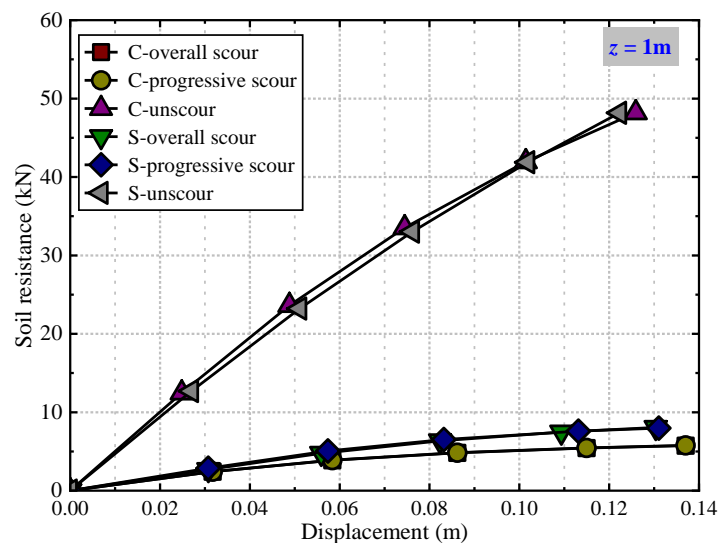


Figure 10. p - y curve at 1 m below the post-scour mudline for the square- and circular-section piles under three scenarios: unscoured, overall scour, and progressive scour.

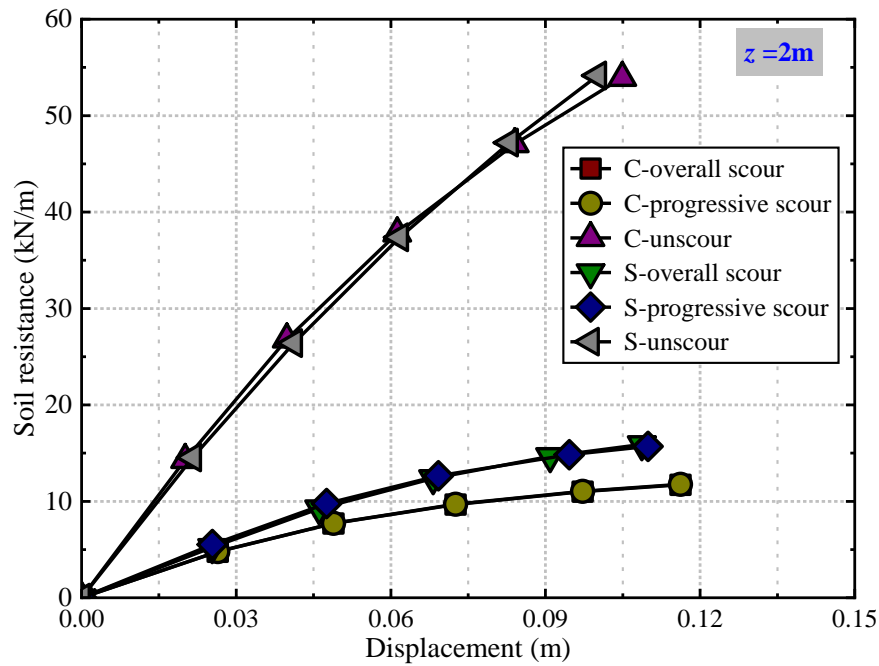


Figure 11. p - y curve at 2m below the post-scour mudline for the square- and circular-section piles under three scenarios: unscoured, overallscour, and progressive scour.

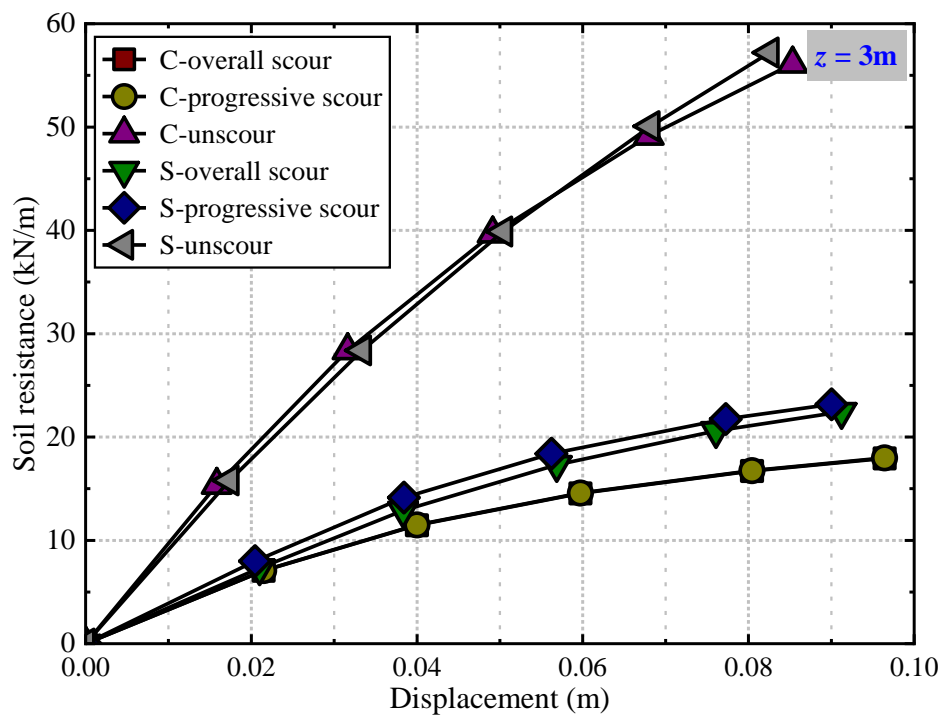


Figure 12. p - y curve at 3 m below the post-scour mudline for the square- and circular-section piles under three scenarios: unscoured, overallscour, and progressive scour.

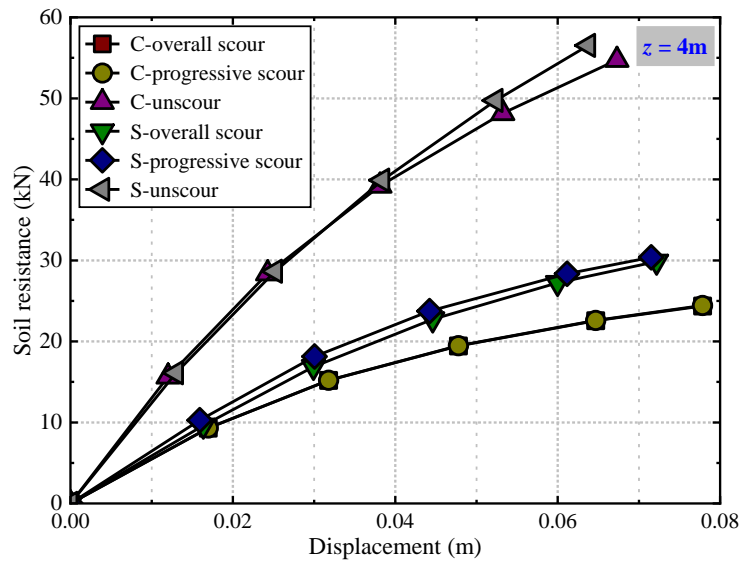


Figure 13. p - y curve at 4m below the post-scour mudline for the square- and circular-section piles under three scenarios: unscoured, overall scour, and progressive scour.

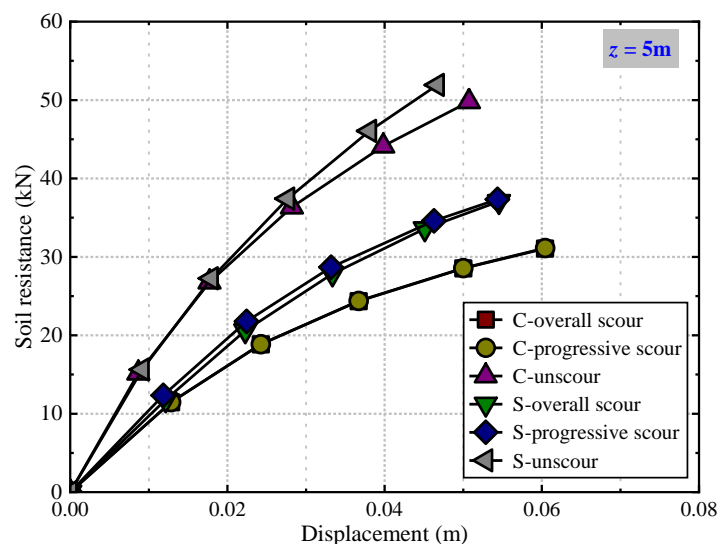


Figure 14. p - y curve at 5 m below the post-scour mudline for the square- and circular-section piles under three scenarios: unscoured, overall scour, and progressive scour.

7. Conclusions

This study established and verified a finite element model through centrifuge tests. Based on the verified finite element model, the research investigated the lateral bearing performance of square and circular pile foundations with equal cross-sections under general scour conditions (overall scour and distribution scour). The analysis addressed pile responses and deformation failure modes of soils around the pile, yielding the following main conclusions:

(1) General scour reduces the lateral bearing capacity for both circular and square cross-section pile foundations. Under no-scour and general scour conditions, square cross-section pile foundations exhibit increases in lateral bearing capacity of 13% and 17.7%, respectively, compared to circular cross-section piles. General scour decreases the effective embedment depth of pile foundations and increases load eccentricity, thereby reducing the wedge-shaped failure zone in soils around the pile, with the depth of the wedge zone shifting deeper into the soil with scour.

(2) In clayey environments, for a specific scour depth, overall scour and distribution scour exert minimal influence on the lateral bearing response of pile foundations, with nearly identical load-displacement relationships, bending moments, and displacement distributions along depth.

(3) When pile foundations bear the same displacement load, bending moment distributions along depth first increase and then decrease. At the same depth, bending moment values under no-scour conditions exceed those under general scour conditions, with this difference becoming more significant as displacement load increases. The depth of maximum bending moment shifts away from the initial mudline with general scour. At the same depth, bending moment values for square cross-section piles surpass those for circular piles with equal cross-sectional areas. Adopting square cross-section pile foundations under scour conditions increases their lateral bearing capacity.

(4) For both circular and square cross-section piles, general scour increases lateral displacement of pile foundations but exerts minimal influence on the depth of the zero-displacement point. Under general scour conditions, the depth of the zero-displacement point for rectangular cross-section pile foundations is shallower than for circular cross-section pile foundations.

(5) At a given depth and lateral displacement, the unscoured case mobilises higher soil reaction than the scoured cases, with the difference diminishing with depth. Overall and progressive scour produce similar p - y responses. The equal-area square pile consistently develops greater soil resistance than the circular pile, indicating improved lateral capacity under all conditions.

Author Contributions: Investigation, L.P.; Data curation, X.D.; Writing—original draft, X.L.; Writing—review & editing, X.L. and Y.L.; Visualization, B.D. and Y.X.; Supervision, B.M., Z.W. and T.L.; Project administration, B.M.; Funding acquisition, B.M. All authors have read and agreed to the published version of the manuscript.

Funding: The work was supported by the National Natural Science Foundation of China (Grant No. 52508378 and 51778227), the Hunan Provincial Natural Science Foundation (2026JJ50476 and 2025JJ60340), Open Research Fund of the Key Laboratory of Mountain Town Construction and New Technology, Ministry of Education (LNTCCMA-20250110), the Scientific Research Fund of the Hunan Provincial Education Department (21A0308).

Data Availability Statement: The datasets presented in this article are not readily available because the data are part of an ongoing study. Requests to access the datasets should be directed to Binhui Ma.

Conflicts of Interest: The authors declare no conflict of interest.

References

1. Cao G, Ding X, Yin Z, Zhou H, Zhou P. A new soil reaction model for large-diameter monopiles in clay. *Comput Geotech.* 2021;137:104311.
2. Li Q, Askarinejad A, Gavin K. Impact of scour on lateral resistance of wind turbine monopiles: an experimental study. *Can Geotech J.* 2021;58(11):1770-82.
3. Peng Y, Liu H, Li C, Ding X, Deng X, Wang C. The detailed particle breakage around the pile in coral sand. *Acta Geotech* 2021;16(6):1971-81.
4. Wang C, Liu H, Ding X, Wang C, Ou Q. Study on the horizontal bearing characteristics of pile foundation in coral sand. *Can Geotech J.* 2021;(ja).
5. Zhu B, Ren J, Yuan S, Zhu J, Yang Q, Gao Y, et al. Centrifuge modeling of monotonic and cyclic lateral behavior of monopiles in sand. *Journal of Geotechnical Geoenvironmental Engineering.* 2021;147(8):04021058.
6. Lagasse PF. Countermeasures to protect bridge piers from scour: Transportation Research Board; 2007.
7. Zhou H, Liu HL, Wang LH, Kong GQ. Finite element limit analysis of ultimate lateral pressure of XCC pile in undrained clay. *Comput Geotech.* 2018;95:240-6. doi: 10.1016/j.compgeo.2017.10.015. PubMed PMID: WOS:000423014600021.
8. Qi C-G, Zheng J-H, Zuo D-J, Liu G-B. Experimental investigation on soil deformation caused by pile buckling in transparent media. *Geotech Test J.* 2018;41(6):1050-62.
9. Li Q, Askarinejad A, Gavin K. The impact of scour on the lateral resistance of wind turbine monopiles: an experimental study. *Can Geotech J.* 2020. doi: 10.1139/cgj-2020-0219.

10. Yuan B, Sun M, Wang Y, Zhai L, Luo Q, Zhang X. Full 3D displacement measuring system for 3D displacement field of soil around a laterally loaded pile in transparent soil. *Int J Geomech* 2019;19(5):04019028.
11. Zhu B, Ren J, Yuan S, Zhu J, Yang Q, Gao Y, et al. Centrifuge modeling of monotonic and cyclic lateral behavior of monopiles in sand. 2021;147(8):04021058.
12. Mohamed YA, Nasr-Allah TH, Abdel-Aal GM, Awad AS. Investigating the effect of curved shape of bridge abutment provided with collar on local scour, experimentally and numerically. *Ain Shams Engineering Journal*. 2015;6(2):403-11. doi: 10.1016/j.asej.2014.10.011.
13. Nasr-Allah TH, Moussa YAM, Abdel-Aal GM, Awad AS. Experimental and numerical simulation of scour at bridge abutment provided with different arrangements of collars. *Alexandria Engineering Journal*. 2016;55(2):1455-63. doi: 10.1016/j.aej.2016.01.021.
14. Namaee Mr, Sui J. Local scour around two side-by-side cylindrical bridge piers under ice-covered conditions. *Int J Sediment Res* 2019;34(4):355-67. doi: 10.1016/j.ijsrc.2018.11.007.
15. Sheppard DM, Melville B, Demir H. Evaluation of Existing Equations for Local Scour at Bridge Piers. *Journal of Hydraulic Engineering*. 2014;140(1):14-23. doi: 10.1061/(asce)hy.1943-7900.0000800.
16. Zubeldia EH, Fournakos G, Rogers BD, Farias MM. Multi-phase SPH model for simulation of erosion and scouring by means of the shields and Drucker-Prager criteria. *Adv Water Resour*. 2018;117:98-114. doi: 10.1016/j.advwatres.2018.04.011.
17. Zou XJ, Cao X, Zhou CL, Zhou M, Zhang XH. Experimental study on the bearing capacity of large-diameter monopile in sand under water flow condition. *Ocean Eng*. 2021;224:108708. doi: ARTN 108708
18. 10.1016/j.oceaneng.2021.108708. PubMed PMID: WOS:000628913000011.
19. Yang X, Zhang C, Huang M, Yuan J. Lateral loading of a pile using strain wedge model and its application under scouring. *Mar Georesour Geotec*. 2017;36(3):340-50. doi: 10.1080/1064119x.2017.1317889.
20. Ma L, Wang L, Guo Z, Jiang H, Gao Y. Time development of scour around pile groups in tidal currents. *Ocean Eng*. 2018;163:400-18. doi: 10.1016/j.oceaneng.2018.06.035.
21. Najafzadeh M, Kargar AR. Gene-Expression Programming, Evolutionary Polynomial Regression, and Model Tree to Evaluate Local Scour Depth at Culvert Outlets. *Journal of Pipeline Systems Engineering and Practice*. 2019;10(3). doi: 10.1061/(asce)ps.1949-1204.0000376.
22. Wang Z, Zhou H, Tong L, editors. *Influence of Scour Depth on Pile Group with Complex Configuration in Clay*. International Conference on Green Building, Civil Engineering and Smart City; 2022: Springer.
23. Al-Mandeel SJ. Behavior of laterally loaded pile group model in sand: King Fahd University of Petroleum and Minerals (Saudi Arabia); 2000.
24. Amini A, Melville BW, Ali TM, Ghazali AH. Clear-Water Local Scour around Pile Groups in Shallow-Water Flow. *Journal of Hydraulic Engineering*. 2012;138(2):177-85. doi: 10.1061/(asce)hy.1943-7900.0000488.
25. Brown D A MC, Reese L C. Lateral load behavior of pile group in sand. *Journal of Geotechnical Engineering*. 1988.
26. Chen Y, Lu F, Namdar A, Cai J. Working Mechanism of Pile Group with Different Pile Spacing in Dense Sand. *Advances in Civil Engineering*. 2019;2019:1-16. doi: 10.1155/2019/5376594.
27. Zhu B, Xiong G, Li T, Liu JC. Centrifuge model tests on laterally loaded piles in sand. *International Journal of Physical Modelling in Geotechnics*. 2016;16(4):160-72. doi: 10.1680/jphmg.15.00023. PubMed PMID: WOS:000388417900002.
28. Cheng X, Fang Z, Li Q, El Naggar MH, Lu D, Du X. Dynamic response of offshore wind turbine supported by suction bucket in clay considering scour. *Ocean Eng*. 2024;313:119414.
29. Li Y, Li Y, Guo Z, Xu Q. Durability of MICP-reinforced calcareous sand in marine environments: Laboratory and field experimental study. *Biogeotechnics*. 2023;1(2):100018.
30. Liang F-Y, Wang Y-Q, Han J. Numerical Analysis of Scouring Effects on the Behavior of Pile Foundations with the Mohr-Coulomb Model. *Condition, Reliability, and Resilience Assessment of Tunnels and Bridges* 2011. p. 82-7.
31. Li F, Han J, Lin C. Effect of Scour on the Behavior of Laterally Loaded Single Piles in Marine Clay. *Mar Georesour Geotec*. 2013;31(3):271-89. doi: 10.1080/1064119x.2012.676157.

32. Wang Z, Zhou H, Sheil B. Effects of scour on the lateral response of piles in sand: centrifuge tests and numerical investigation. *Acta Geotech* 2025:1-20.
33. Wang C, Liang F, Yu X. Experimental and numerical investigations on the performance of sacrificial piles in reducing local scour around pile groups. *Nat Hazards*. 2016;85(3):1417-35. doi: 10.1007/s11069-016-2634-0.
34. Aamir M, Ahmad Z. Review of literature on local scour under plane turbulent wall jets. *Phys Fluids*. 2016;28(10). doi: 10.1063/1.4964659.
35. Alemi M, Maia R. Numerical Simulation of the Flow and Local Scour Process around Single and Complex Bridge Piers. *Int J Civ Eng*. 2016;16(5):475-87. doi: 10.1007/s40999-016-0137-8.
36. Ciancimino A, Jones L, Sakellariadis L, Anastasopoulos I, Foti S. Experimental assessment of the performance of a bridge pier subjected to flood-induced foundation scour. *Geotechnique*. 2021:1-18.
37. Biao L, Wen-Gang Q, Yifa W, Fu-Ping G, Shun-Yi W. Scour-induced unloading effects on lateral response of large-diameter monopiles in dense sand. *Comput Geotech*. 2024;174. doi: 10.1016/j.compgeo.2024.106635.
38. He B, Lai Y, Wang L, Hong Y, Zhu R. Scour Effects on the Lateral Behavior of a Large-Diameter Monopile in Soft Clay: Role of Stress History. *Journal of Marine Science and Engineering*. 2019;7(6). doi: 10.3390/jmse7060170.
39. Y K, Q W, G.B L. Measures to resist flood disaster of bridge gossing. *Journal of railway engineering society*. 1998.
40. Liang F, Zhang H, Huang M. Influence of flood-induced scour on dynamic impedances of pile groups considering the stress history of undrained soft clay. *Soil Dyn Earthq Eng*. 2017;96:76-88. doi: 10.1016/j.soildyn.2017.02.009.
41. 2GEO AJAR. Geotechnical and foundation design considerations. API Washington, DC; 2011.
42. Shafts D. Construction Procedures and Design Methods. US Department of Transportation, Federal Highway Administration, Volumes I and II. 1999.
43. Qi WG, Gao FP, Randolph MF, Lehane BM. Scour effects on p-y curves for shallowly embedded piles in sand. *Geotechnique*. 2016;66(8):648-60. doi: 10.1680/jgeot.15.P.157.
44. Chortis G, Askarinejad A, Prendergast LJ, Li Q, Gavin K. Influence of scour depth and type on p-y curves for monopiles in sand under monotonic lateral loading in a geotechnical centrifuge. *Ocean Eng*. 2020;197. doi: 10.1016/j.oceaneng.2019.106838.
45. Wang Z, Zhou H, Franza A, Liu H. Numerical evaluation of scour effects on lateral behavior of pile groups in clay. *Comput Geotech*. 2022;150:104913.
46. Wang Z, Zhou H, Sheil B, Liu H, Wang C. Numerical investigation of the lateral response of pile groups in sand under local scour conditions. *Comput Geotech*. 2023;159:105435.
47. Lin C. Case history analysis of bridge failures due to scour. *Comput Geotech*. 2013.
48. Lin C, Han J, Bennett C, Parsons RL. Analysis of laterally loaded piles in soft clay considering scour-hole dimensions. *Ocean Eng*. 2016;111:461-70. doi: 10.1016/j.oceaneng.2015.11.029.
49. Ilyas T, Leung CF, Chow YK, Budi4 aSS. Centrifuge Model Study of Laterally Loaded Pile Groups in Clay. *J Geotech Geoenviron*. 2004.
50. Wang L, Wang H, Zhu B, Hong Y. Comparison of monotonic and cyclic lateral response between monopod and tripod bucket foundations in medium dense sand. *J Ocean Engineering*. 2018;155:88-105.
51. Truong P, Lehane BM. Effects of pile shape and pile end condition on the lateral response of displacement piles in soft clay. *Geotechnique*. 2018;68(9):794-804. doi: 10.1680/jgeot.16.P.291. PubMed PMID: WOS:000440975400004.

Disclaimer/Publisher's Note: The statements, opinions and data contained in all publications are solely those of the individual author(s) and contributor(s) and not of MDPI and/or the editor(s). MDPI and/or the editor(s) disclaim responsibility for any injury to people or property resulting from any ideas, methods, instructions or products referred to in the content.